Semnan University

Progress in Physics of Applied Materials

journal homepage: https://ppam.semnan.ac.ir/

Hydrothermal synthesis of Fe_3O_4-ZnO nanocomposites for removing fluoride from water

Salimeh Kimiagar [a,b*], Hoda Mirazimi[c]

[a]*Nanophysics Research Lab (NRL), Department of Physics, Central Tehran Branch, Islamic Azad University, Tehran, Iran*
[b]*Physics Department, Pontifical Catholic University of Rio de Janeiro (PUC-Rio), Rio de Janeiro, 22451-900, Brazil*
[c]*Department of Physics, Central Tehran Branch, Islamic Azad University, Tehran, Iran*

ARTICLE INFO

Article history:
Received: 17 March 2024
Revised: 8 May 2024
Accepted: 19 May 2024

Keywords:
Hydrothermal
Fluoride
Water pollution
Fe_3O_4-ZnO
Magnetic nanoparticle

ABSTRACT

Numerous nations are grappling with a significant challenge related to the prevalence of fluorosis, stemming from elevated fluoride levels in drinking water. This study aims to investigate avenues for eliminating fluoride from water solutions utilizing cost-effective, nontoxic, and readily available adsorbents. In this research, Fe_3O_4-ZnO nanocomposites were synthesized using the hydrothermal method which is a simple and environmentally friendly method that can be easily performed on a large scale. X-Ray diffraction analysis and Williamson-Hall plots were used to study the phase purity, crystallite size, strain, lattice constant, and d-spacing of the samples. The morphology of the samples was investigated through Scanning Electron Microscopy and Transmission Electron Microscope. The formation of nanocomposites was investigated by Vibrating Sample Magnetometer analyses. The Fe_3O_4-ZnO nanocomposites were then used for fluoride removal from water. The results showed that Fe_3O_4-ZnO-2 could absorb 78% of the fluoride after 80 minutes. Then, Fe_3O_4-ZnO-2 was collected using a magnet within 50 seconds. These results are important in that, despite their simplicity, it has no side effects on the environment.

1. Introduction

Water is a fundamental resource essential for sustaining life on Earth and supporting diverse ecosystems. However, the increasing human population, urbanization, and industrialization have exerted immense pressure on water resources. One of the most pervasive forms of water pollution is chemical contamination, which arises from industrial discharges, agricultural runoff, and improper disposal of household chemicals [1, 2].

Fluoride contamination in water sources has emerged as a significant environmental and public health concern, particularly in regions where natural fluoride levels exceed recommended limits or anthropogenic activities contribute to elevated concentrations [3, 4]. Excessive fluoride levels in drinking water pose various health risks, ranging from dental and skeletal fluorosis to neurological disorders and developmental abnormalities. Dental fluorosis, characterized by enamel discoloration and dental erosion, is a common manifestation of chronic fluoride exposure during tooth development, particularly in children. Skeletal fluorosis, on the other hand, involves the accumulation of fluoride in bones and joints, resulting in stiffness, pain, and skeletal deformities [5, 6]. Several techniques such as activated alumina, ion exchange, reverse osmosis, coagulation, membrane process, and adsorption can be used for de-fluoridation [7-12]. Each method has its advantages and disadvantages in terms of cost, effectiveness, and practicality. The adsorption method is the widely used method for fluoride elimination because it is an effective, convenient, low cost, and environmentally compatible technology [13]. Materials containing small and low volume pores that increase the surface area are important for adsorption and chemical reactions. The specific surface area

* Corresponding author.
E-mail address: s_kimiagar@iauctb.ac.ir

Cite this article as:
Kimiagar, S. and Mirazimic, H., 2024. Hydrothermal synthesis of Fe_3O_4-ZnO nanocomposites for removing fluoride from water. *Progress in Physics of Applied Materials*, 4(1), pp.83-91. DOI: 10.22075/PPAM.2024.33571.1092

and pore structure are mainly related to physical adsorption properties.

Fe_3O_4 nanoparticles, commonly known as magnetite, possess intrinsic magnetic properties, enabling their facile separation from aqueous solutions using external magnetic fields. Large surface area-to-volume ratios, tunable surface chemistry, surface complexation, ion exchange processes, and the potential for magnetic separation, make them highly effective in adsorbing fluoride ions from water [14-18]. Moreover, the presence of Fe_3O_4 nanoparticles can induce the formation of iron hydroxide species on their surfaces, which further enhances fluoride removal via co-precipitation and surface precipitation mechanisms. *ZnO* nanoparticles offer distinct advantages for fluoride removal, which include high surface reactivity, photocatalytic activity, and ease of synthesis. *ZnO* nanoparticles possess a wide bandgap and exhibit photocatalytic properties under UV irradiation, enabling the degradation of organic contaminants and the regeneration of adsorption sites for fluoride ions. Furthermore, the presence of surface hydroxyl groups on *ZnO* nanoparticles facilitates fluoride adsorption through hydrogen bonding and surface complexation reactions, leading to efficient removal from water matrices [19, 20].

In this paper, we provide a comprehensive overview of the utilization of Fe_3O_4 and *ZnO* nanocomposites for fluoride removal from water sources. Furthermore, we discuss the factors influencing the adsorption performance of Fe_3O_4 and *ZnO* nanoparticles, such as nanoparticles morphology. We aim to elucidate the efficacy and potential applications of Fe_3O_4 and *ZnO* nanocomposites for fluoride remediation in water treatment processes. By highlighting the advantages and challenges associated with nanoparticle-based approaches, we seek to contribute to the development of sustainable and cost-effective solutions for mitigating fluoride contamination and ensuring access to safe drinking water for communities worldwide.

2. Experimental details and Characterization

All materials in these experiments were purchased from Merck Company. Iron (II) chloride tetrahydrate ($FeCl_2.4H_2O$, molecular weight:198.81, purity ≥99.0 %), Iron (III) chloride ($FeCl_3.6H_2O$, molecular weight:162.20, purity ≥99.0 %), Ethanol (C_2H_5OH, purity (GC), ≥ 99.9 %), Sodium hydroxide (*NaOH*) 97%, zinc acetate $ZnC_4H_6O_4$ (Molar mass: 183.48 g/mol, Density: 1.74 g/cm^3).

Synthesis of Fe_3O_4: 2.4 g of $FeCl_2\ 4\ H_2O$, 6.16 g of $FeCl_3\ 6\ H_2O$, were mixed with 200 mL of doubly distilled (DI) water. 12 g of Sodium hydroxide (*NaOH*) were added to the solution drop by drop until the black solution formed. Then by a magnet Fe_3O_4 nanoparticles collected and washed with ethanol and DI water (×2) and dried at temperature 60 ˚C.

Synthesis of ZnO*:* Zinc oxide (*ZnO*) was prepared by hydrothermal method. Solution one: 4 g of *NaOH* were added to 100 mL of DI water. Solution two: 8 g of zinc acetate ($ZnC_4H_6O_4$) were added to 50 mL of DI water at temperature 50 ˚C while stirred. Then the solution one was slowly added to solution two drop by drop, till white solution color was formed. Then the final solution transferred to a stainless-steel autoclave reactor with a 200 mL Teflon lined hydrothermal autoclave. The reaction was performed at 180 °C for 18 h. After cooling down to room temperature, the achieved powder was washed with ethanol and DI water (twice) and dried in a vacuum oven at 60 °C.

Synthesis of Fe_3O_4-ZnO core–shell: Here, two nanocomposites Fe_3O_4-*ZnO*-1 and Fe_3O_4-*ZnO*-2 are prepared with different weight percentages of *ZnO* (0.5 and 1 g). For Fe_3O_4-*ZnO*-1, 0.7 g of iron oxide and 0.5 g of zinc oxide were dispersed in 150 mL of DI water. Then the solution transferred to a 200 m stainless-steel Teflon lined hydrothermal autoclave reactor. The reaction was performed at 180°C for 15 h. After cooling down to room temperature, the achieved powder was washed with DI water (twice) and dried in a vacuum oven at 60 °C. The resulting powder labeled Fe_3O_4-*ZnO*-1. The same process was repeated with 1 g *ZnO* and the sample marked as Fe_3O_4-*ZnO*-2.

Characterization: In order to identify the phase purity and crystalline nature of the samples, X-ray diffraction (XRD) model (SIE:ID3003, Germany) with monochromatic Cu Kα (λ = 1.54 Å) was used. The analysis of the surface morphologies of the samples was performed with a Philips XL-30 scanning electron microscope (SEM) and transmission electron microscopy (TEM, Tecnai 20 operating 200 kV). Magnetization measurements were carried out with a vibrating sample magnetometer (VSM) (Magnetic Daneshpajoh Kashan, model MDKB) to study magnetic properties of the samples under magnetic fields up to 10KG (1T) at room temperature. Absorption spectrum was performed with a UV-Vis spectrophotometer (lambada 750, Germany).

3. Results and discussion

3.1. Nanocomposites structural analysis

The crystallinity and phase of the synthesized samples using diffraction patterns are depicted in Figure 1. In Figure 1a, all peaks of the Fe_3O_4 XRD pattern align with those in the (JCPDS 19-0629) database. Notably, distinct diffraction peaks are evident at angles corresponding to the (200), (311), (400), (422), (511), and (440) crystallographic face-centered cubic inverse spinel structure. The space group of the Fe_3O_4 (iron (II, III) oxide) crystal structure is Fd-3m (No. 227). This space group represents a face-centered cubic lattice with a space-filling motif of Fe atoms and O atoms. The presence of sharp peaks indicates a well-defined crystal structure without any impurities. Figure 1b showcases *ZnO* exhibiting the wurtzite phase, with all diffraction peaks matching the reported data in (JCPDS 36-1451). No additional characteristic peaks besides *ZnO* were observed. The space group of zinc oxide (ZnO) is P63mc (No. 186). This space group represents a hexagonal crystal lattice with a motif of alternating zinc and oxygen atoms. Lattice parameters are a= 3.48(Å) and c= 1.29(Å). Notably, there is a strong preferential growth along the (101) direction, corresponding to the wurtzite phase of *ZnO*. Figure 1c depicts the XRD pattern of the samples. It is noted that in Fe_3O_4-*ZnO*-2, the increased weight of zinc oxide compared with Fe_3O_4-*ZnO*-1, results in higher intensity peaks associated with zinc oxide, while the intensity of Fe_3O_4 peaks decreases. It suggests that ZnO is the dominant

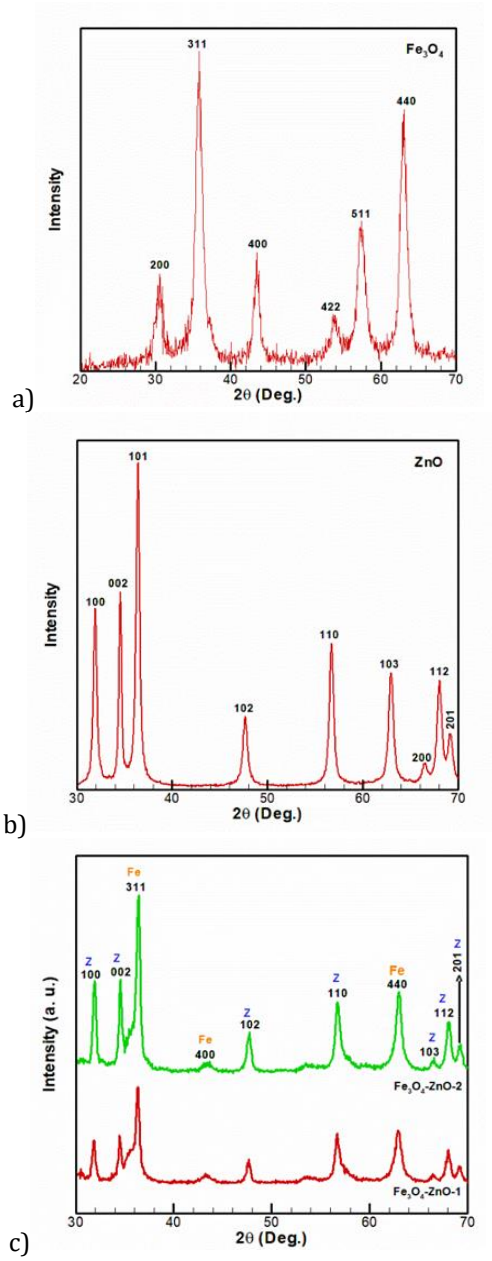

Fig. 1. XRD pattern of a) Fe_3O_4 , b) *ZnO,* and c) Fe_3O_4-*ZnO*-1 and Fe_3O_4-*ZnO*-2 nanocomposites. Fe symbolized to Fe_3O_4 peaks and Z is signified *ZnO* peaks.

in the nanocomposite. Fe symbolized to Fe_3O_4 peaks and Z is signified *ZnO* peaks.

The interplanar spacing '*d*' and lattice parameter '*a*' for Fe_3O_4, *ZnO*, Fe_3O_4-*ZnO*-1, and Fe_3O_4-*ZnO*-2 are calculated through Equation (1-3). Where 'θ' is Bragg angle for reflection through (311) plane which is most intense refraction of Fe_3O_4, Fe_3O_4-*ZnO*-1, and Fe_3O_4-*ZnO*-2. For ZnO the intense refraction is (101) plane. '*n*' is the order of diffraction and λ is the wavelength of used X-rays (1.54 Å). The calculation results are collected in Table 1.

$$2d\sin\theta = n\lambda \tag{1}$$

$$a = d\sqrt{h^2 + k^2 + l^2} \tag{2}$$

$$\frac{1}{d^2} = \frac{4}{3}\left(\frac{h^2 + hk + k^2}{a^2}\right) + \frac{l^2}{c^2} \tag{3}$$

The XRD patterns presented the sharp reflections consistent to each plane which is attributed to long range ordering. Here, the crystallite size is calculated through Williamson-Hall (W-H) equation (4) [20]:

$$\beta\cos\theta = 4\epsilon\sin\theta + k\lambda/D \tag{4}$$

Where, β and θ are full width at half maximum (FWHM) and peak position in radians corresponding to each reflection plane, respectively. k is shape parameter which has value of 0.9 for spherical morphological nanoparticles. ε denotes the strain formed in crystal lattice. The graph of $\beta\cos\theta$ versus $4\sin\theta$ is known as W-H plot which gives the values of crystallite size and induced strain within the crystal. Here, the crystallite size is estimated through intercept on $\beta\cos\theta$ axes whereas the induced strain is the slope of W-H curve in Figure 2. The average crystallite size (D) and the average of lattice strain (ε) for all samples are presented in Table 1. The magnitude of the strain formed in a crystal lattice depends on the specific materials involved, the growth conditions, the presence of defects, and external factors such as temperature and stress. Large amount of strain for the samples would be due to hydrothermal temperature and defects [21]. Though, the average particle was observed to be larger in comparison to crystallite size calculated from W-H plot method. The difference is due to the fact that one particle may contain many crystallites.

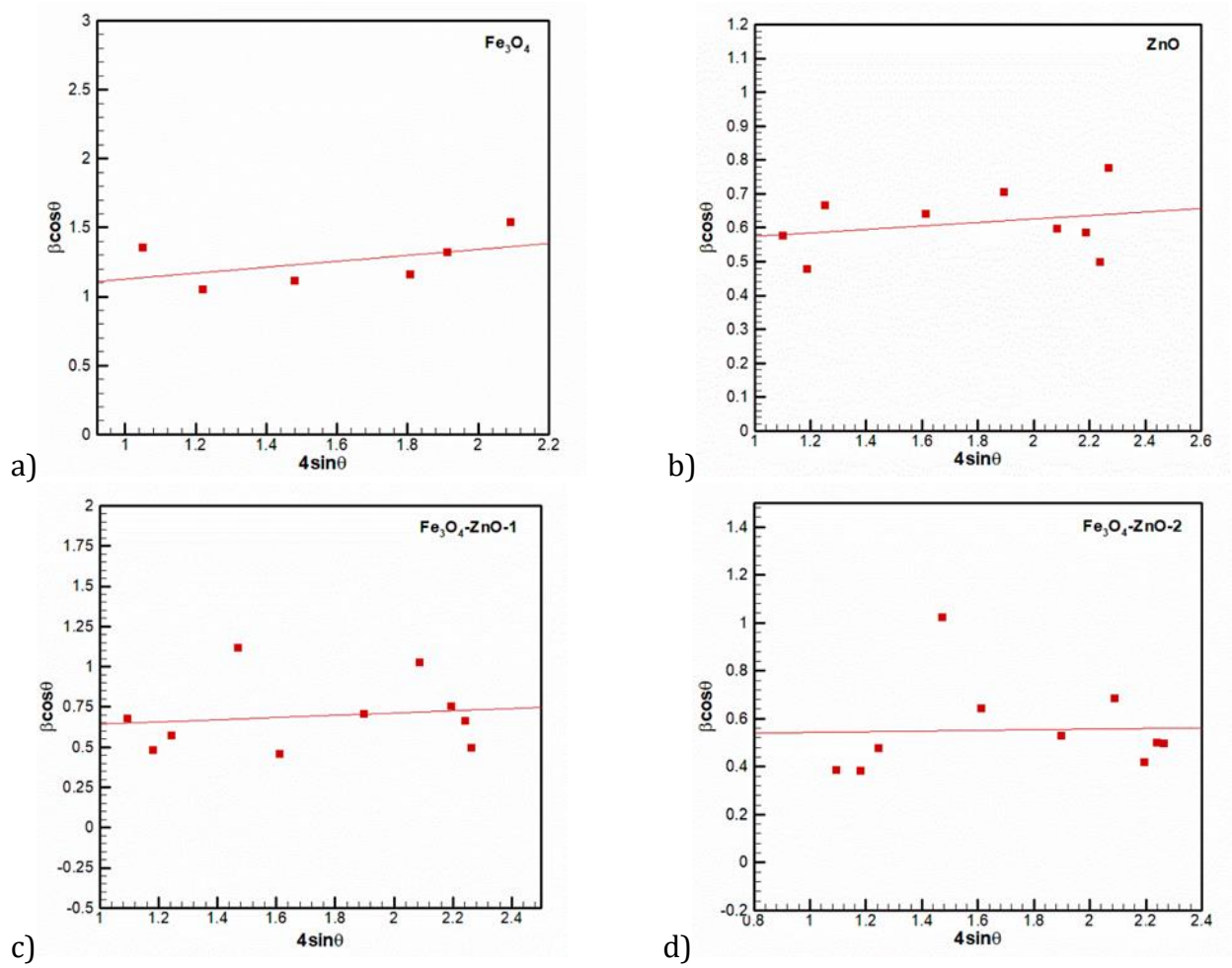

Fig. 2. Williamson-Hall plots for a) Fe_3O_4, b) *ZnO*, c) Fe_3O_4-*ZnO*-1, and d) Fe_3O_4-*ZnO*-2 nanocomposites.

Table 1. calculated data from XRD for the samples.

Sample	2θ(Degree)	Plane	ε±0.003	D(Å)±4.55	d-spacing (Å)±0.015	a (Å)±2.008
Fe_3O_4	35.9	(311)	0.075	15	2.5	8.29
ZnO	36.5	(101)	0.052	26	2.46	3.48
Fe_3O_4-*ZnO*-1	36.4	(311)	0.007	24	2.47	8.19
Fe_3O_4-*ZnO*-2	36.4	(311)	0.001	26	2.47	8.19

Fig. 3a shows the magnetization loop for magnetite nanocomposites at room temperature and Figure 3b is enlarge spectrum of Figure 3a. The magnetic hysteresis curves demonstrate superparamagnetic behavior for Fe_3O_4-*ZnO*-1 and Fe_3O_4-*ZnO*-2. These samples exhibit a narrow hysteresis curve characterized by low coercivity and retentivity values (Table 2). Size-dependent variations in coercivity arise from complex interplays among shape anisotropy, surface effects, finite size effects, interface effects, and the presence of defects and dislocations in nanoscale magnetic materials [22]. According to VSM results, the coercivity (H_c), representing the field necessary for magnetization, is 6 Oe for Fe_3O_4, and 1 Oe for Fe_3O_4-*ZnO*-1 and Fe_3O_4-*ZnO*-2. Retentivity (M_R), indicating the field required for demagnetization is lower due to the superparamagnetic nature of the samples, making them prone to lose magnetization easily. The saturation magnetization values (Table 2) suggest that beyond this threshold, the samples cannot be further magnetized. This decreasing of *Ms* value is attributed to the incorporation of nonmagnetic *ZnO* into Fe_3O_4 structure. The variation of saturation magnetization with particle size in magnetic materials arises from a combination of finite size effects, surface and interface contributions, shape anisotropy, magnetic domain structure, and the presence of surface oxidation and defects. It seems interface effects and the presence of defects in the samples are responsible for variation of H_C and M_S [23]. Additional significant magnetic parameter is squareness ratio (S) which is defined as the ratio of remanence magnetization (M_R) to saturation magnetization (M_S). It is a measure of the shape of hysteresis loop in a magnetic material. It quantifies the degree of squareness or rectangularity of the loop, which represents the material's magnetic behavior under the influence of an external magnetic field. It shows values between the squareness of superparamagnetic material (M_R/M_S = 0) and the square loop (i.e., M_R/M_S = 1) [24]. A squareness ratio of 1 indicates a perfectly square hysteresis loop, where the material exhibits ideal ferromagnetic behavior, reaching full saturation with no residual magnetization when the applied field is removed. A squareness ratio below 0.5 suggests the presence of a small,

single-domain assembly of spherical particles with random orientation. Lower values typically indicate larger particles and the formation of domain walls.

The values of S for different samples are in Table 2. Anisotropy constant (K) calculated using the relation (5) [25]:

$$K = (Ms \times Hc)/0.96 \quad (5)$$

The values of anisotropy constant are also listed in Table 2. It reveals that the anisotropy constant is decreasing for the nanocomposites [24]. Thus, decrement in magnetization as well as coercivity was observed with enhancement of ZnO in nanocomposites. Analysis of the hysteresis loops reveals that the magnetite samples possess characteristics of a soft magnet, being readily magnetized and demagnetized.

The SEM micrographs of Fe_3O_4 and ZnO nanoparticles are shown in Figure 4. In Figure 4a the morphology of Fe_3O_4 is observed to be agglomerated spherical-shaped [26]. The agglomeration in magnetic nanoparticles is owing to magnetic dipole-dipole interactions between them. Similar agglomerated morphology for magnetic nanoparticles was reported in literature [27]. The SEM image for ZnO, which consists of pseudo-spheres, and uniform particles is shown in Figure 4b.

The SEM images of Fe_3O_4-ZnO-1 and Fe_3O_4-ZnO-2 are shown in Figure 5. In sample Fe_3O_4-ZnO-1, which has less ZnO, spherical Fe_3O_4 nanoparticles are dominate, while in sample Fe_3O_4-ZnO-2, due to the increase in zinc oxide, more pseudo-spheres nanoparticles of ZnO are observed.

TEM images of the samples are presented in Figure 6. More spherical nanoparticles can be observed for Fe_3O_4-ZnO-1(Figure 6a) while for Fe_3O_4-ZnO-2 nanocomposites quasi-spherical nanoparticles predominant (Figure 6b).

Table 2. values of magnetic parameters for Fe_3O_4 , Fe_3O_4-ZnO-1, and Fe_3O_4-ZnO-2 nanocomposites.

Sample	H_C (Oe)	Retentivity (M_R), (emu/g)	Saturation (M_S) (emu/g)	$S=M_R/M_S$	K(erg/g)
Fe_3O_4	6	6	52	0.12	325
Fe_3O_4-ZnO-1	1	4.5	27	0.16	28
Fe_3O_4-ZnO-2	1	2.5	17	0.15	17.7

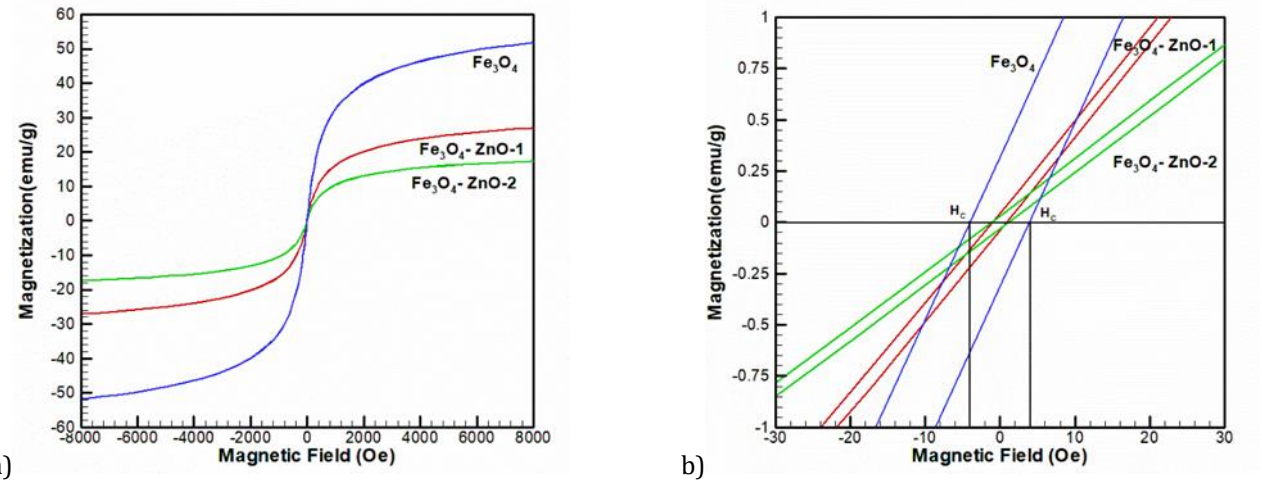

a) b)

Fig. 3. Vibrating sample magnetometer analysis of a) the samples and b) enlarge spectrum of the VSM.

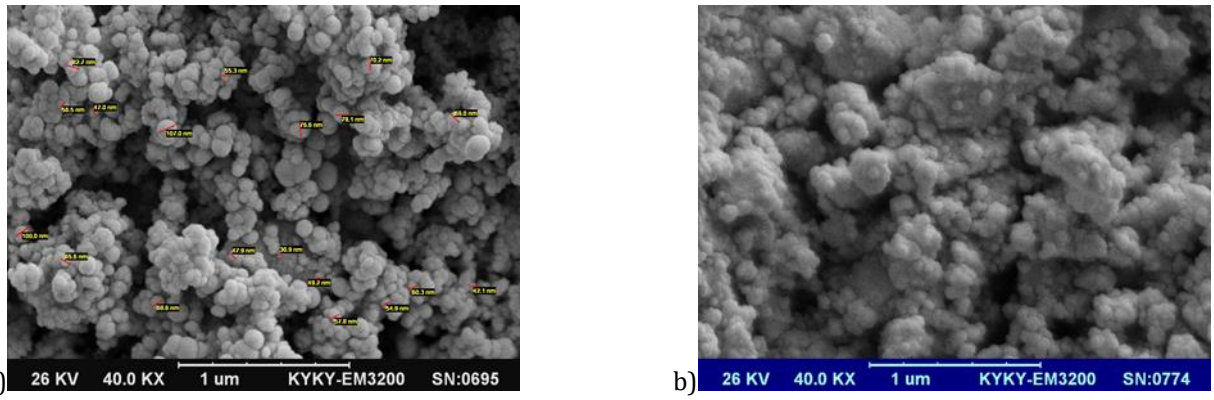

a) b)

Fig. 4. SEM images of a) Fe_3O_4 and b) ZnO.

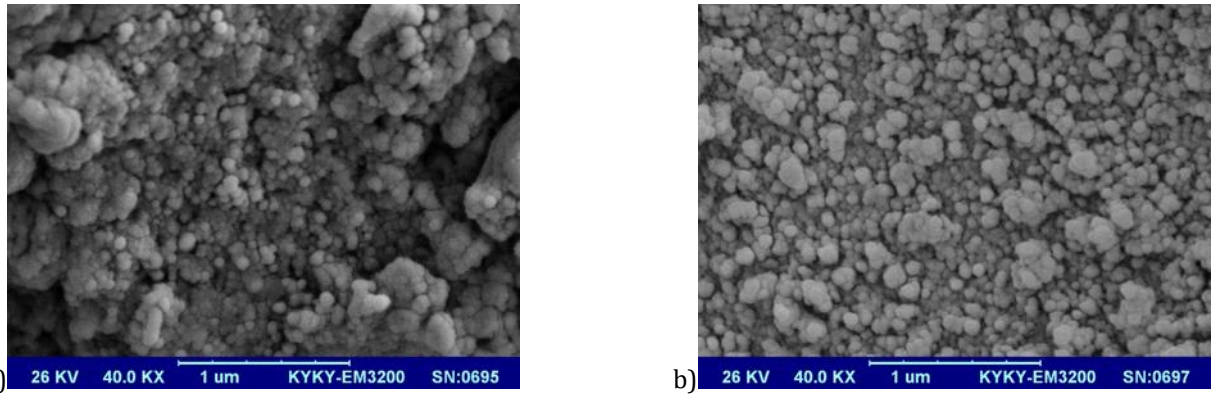

Fig. 5 SEM images of a) Fe_3O_4-ZnO-1 and b) Fe_3O_4-ZnO-2.

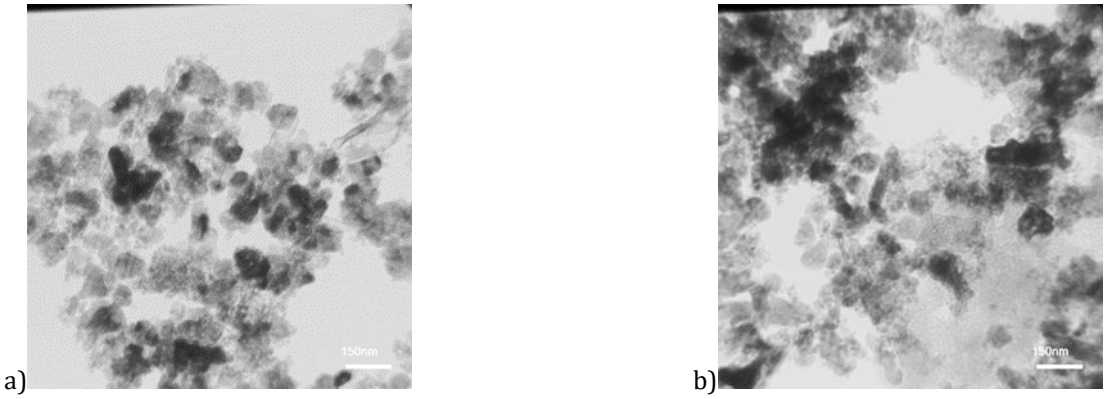

Fig. 6 TEM images of a) Fe_3O_4-ZnO-1 and b) Fe_3O_4-ZnO-2.

3.2. Adsorption Measurements

To examine the effectiveness of nanocomposites as adsorbents for eliminating fluoride from water, an adsorption experiment was conducted. Initially, 1 mg of fluoride was introduced into 100 mL of DI water. Subsequently, 0.1 mg of the Fe_3O_4-ZnO-1 nanocomposites were introduced into the solution. The absorbance of the solution was measured and labeled as "Dark", with the absorbance peak of fluoride being observed at 380 nm. The setup was then subjected to radiation of a 12 W UV light at a distance of 20 cm (Figure 7). The space where the sample is under UV radiation is completely covered so that no other light enters and only the UV effect remains. Absorbance readings were recorded from t=10-80 minutes for both Fe_3O_4-ZnO-1 and Fe_3O_4-ZnO-2 nanocomposites (Figure 8). The decrease in the absorbance peak of fluoride is evident, indicating its successful removal. This reduction for Fe_3O_4-ZnO-2 (Figure 8a) is more than Fe_3O_4-ZnO-1 (Figure 8b) illustrating Fe_3O_4-ZnO-2 is more effective in fluoride absorption.

The removal percentage of fluoride was calculated as the ratio of difference in fluoride concentration before and after adsorption ($C_0 - C_e$) to the initial concentration of the fluoride (C_0) and by using equation:

$$Removal(\%) = \frac{(C_0 - C_e) \times 100}{C_0} \quad (6)$$

Fig. 9 shows the effect of removal of the initial fluoride concentration by Fe_3O_4-ZnO-1 and Fe_3O_4-ZnO-2 nanocomposites. The studies were carried out at different contact time and room temperature. Longer irradiation times allow more photons to be absorbed by the photocatalyst, resulting in the generation of a greater number of electron-hole pairs. This can enhance the photocatalytic activity by increasing the availability of active species for the desired reactions. The results showed that the percentage of removal increase up to 54% and 78% for Fe_3O_4-ZnO-1 and Fe_3O_4-ZnO-2 nanocomposites, respectively. The time for collection of Fe_3O_4-ZnO-1 and Fe_3O_4-ZnO-2 nanocomposites from water (using H=1 T) was 30 and 50 S, respectively.

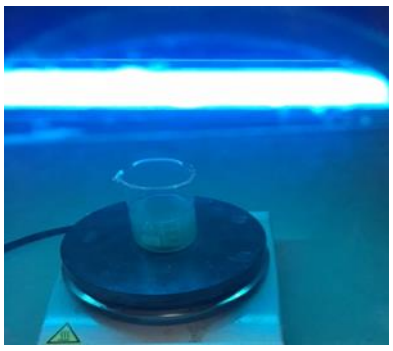

Fig. 7. Adsorption measurements set up.

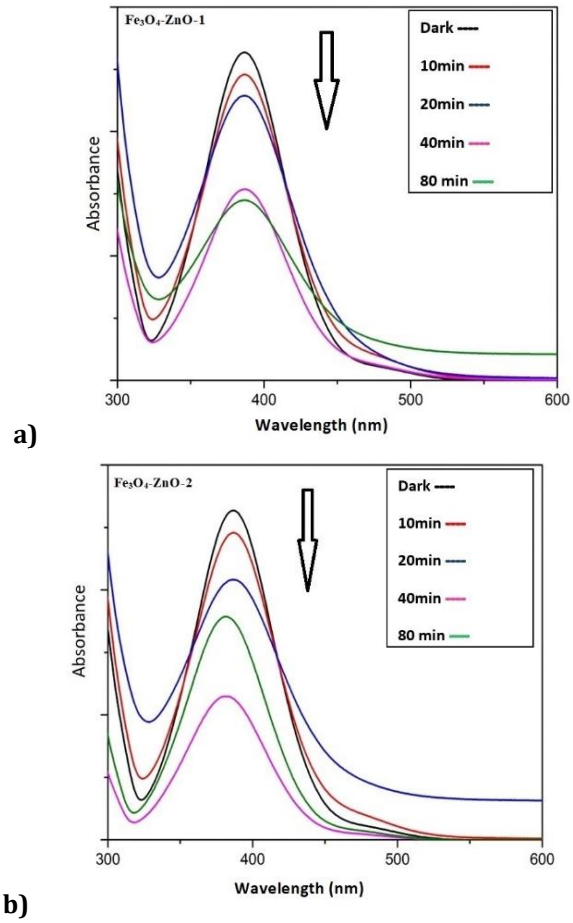

Fig. 8. Absorbance of fluoride by a) Fe_3O_4-ZnO-1 and b) Fe_3O_4-ZnO-2.

Magnetic nanoparticles can be functionalized or modified to attract and bind fluoride ions from water through physical adsorption, in which fluoride ions adhere to the surface of the nanoparticles due to weak forces such as van der Waals interactions or electrostatic attractions. The magnetic property of the nanoparticles allows to easy separation from the water using a magnetic field after adsorption. Therefore, while physical adsorption is likely a significant mechanism in the removal of fluoride using magnetic nanoparticles, the presence of chemical functionalization or other factors could introduce additional mechanisms such as chemical absorption or ion exchange.

In some chemical absorption processes, the surface of magnetic nanoparticles (such as Fe_3O_4) may undergo chemical transformations that could potentially affect their magnetic properties. For instance, if the nanoparticles are involved in a chemical reaction where the iron ions (Fe) on the surface are altered or if a coating material is added that alters the magnetic behavior, it might interfere with their magnetic response. In such cases, the magnetic separation efficiency might be reduced because the altered nanoparticles may not respond as strongly to the magnetic field. However, the extent to which this occurs depends on the specifics of the chemical reaction and the resulting changes in the magnetic properties of the nanoparticles. Since after the removal of fluoride from water, magnetic nanocomposites were quickly (< 1 Min.) separated from water, it can be concluded that their magnetic properties have not decreased, meaning that the absorption of fluoride has been physical.

In applications where maintaining the magnetic response of the nanoparticles is crucial for efficient separation, it is essential to consider factors such as the choice of coating materials, reaction conditions, and post-treatment processes to minimize any adverse effects on the magnetic properties. Additionally, alternative separation methods might be explored if magnetic separation becomes less effective due to changes in the nanoparticles' properties.

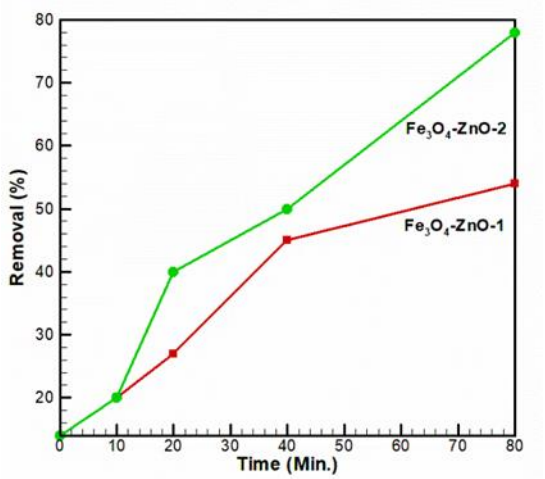

Fig. 9. Removal efficiency of fluoride by Fe_3O_4-ZnO-1 and Fe_3O_4-ZnO-2 nanocomposites.

4. Conclusion

Nowadays, the presence of pollutants in water resources is the greatest concern and has attracted growing attention hence, excessive amounts of pollutants such as fluoride should be removed from drinking water and industrial wastewater. Conventional water treatment processes cannot completely remove extra fluoride from aqueous water bodies, while adsorption is a promising, effective and simple method for this purpose. On this basis, the low-cost, safe, non-toxic, and easily available Fe_3O_4-ZnO nanocomposites were synthesized using the hydrothermal method. XRD showed face-centered cubic inverse spinel structure and the wurtzite phase for Fe_3O_4 and ZnO, respectively. The average of lattice strain (ε) decreased for the Fe_3O_4-ZnO. It can be attributed to various factors such as stress relaxation, diffusion of atoms, plastic deformation, and grain growth. VSM analysis proved the formation of magnetite nanocomposites. The Fe_3O_4-ZnO-1 and Fe_3O_4-ZnO-2 nanocomposites have been used for the quantitative elimination of fluoride from water. The highest removal efficiency (78%) was obtained for 0.1 mg of Fe_3O_4-ZnO-2 and 1 mg of fluoride in 100 mL of DI water after 80 minutes. In comparison, the efficiency of Fe_3O_4-ZnO-1 with a lower amount of ZnO was 54% at the same condition. A magnet could easily separate these nanocomposites from water in less than one minute. The overall results indicated that the

nanocomposites can be used as an effective and suitable absorbance ability method for the removal of fluoride from water sources.

Acknowledgements

This work is supported by Islamic Azad University, Central Tehran Branch.

Conflicts of Interest

The author declares that there is no conflict of interest regarding the publication of this article.

References

[1] Walker, D.B., Baumgartner, D.J., Gerba, C.P. and Fitzsimmons, K., 2019. Surface water pollution. In Environmental and pollution science (pp. 261-292). Academic Press.

[2] Karn, S.K. and Harada, H., 2001. Surface water pollution in three urban territories of Nepal, India, and Bangladesh. Environmental management, 28, pp.483-496.

[3] Roy, S. and Dass, G., 2013. Fluoride contamination in drinking water–a review. Resour. Environ, 3(3), pp.53-58.

[4] Vithanage, M. and Bhattacharya, P., 2015. Fluoride in the environment: sources, distribution and defluoridation. Environmental Chemistry Letters, 13, pp.131-147.

[5] Kumar, P.S., Suganya, S., Srinivas, S., Priyadharshini, S., Karthika, M., Karishma Sri, R., Swetha, V., Naushad, M. and Lichtfouse, E., 2019. Treatment of fluoride-contaminated water. A review. Environmental Chemistry Letters, 17, pp.1707-1726.

[6] Shaji, E., Sarath, K.V., Santosh, M., Krishnaprasad, P.K., Arya, B.K. and Babu, M.S., 2024. Fluoride contamination in groundwater: A global review of the status, processes, challenges, and remedial measures. Geoscience Frontiers, 15(2), p.101734.

[7] Kumar, A., Balouch, A. and Abdullah, 2021. Remediation of toxic fluoride from aqueous media by various techniques. International Journal of Environmental Analytical Chemistry, 101(4), pp.482-505.

[8] Ghorai, S. and Pant, K.K., 2005. Equilibrium, kinetics and breakthrough studies for adsorption of fluoride on activated alumina. Separation and purification technology, 42(3), pp.265-271.

[9] Damtie, M.M., Woo, Y.C., Kim, B., Hailemariam, R.H., Park, K.D., Shon, H.K., Park, C. and Choi, J.S., 2019. Removal of fluoride in membrane-based water and wastewater treatment technologies: Performance review. Journal of environmental management, 251, p.109524.

[10] Sandoval, M.A. and Domínguez-Jaimes, L.P., 2024. Fluoride removal from drinking water by electrocoagulation process: recent studies, modeling, and simulation through computational fluid dynamics approach. In Advances in Drinking Water Purification (pp. 163-179). Elsevier.

[11] Grzegorzek, M., Majewska-Nowak, K. and Ahmed, A.E., 2020. Removal of fluoride from multicomponent water solutions with the use of monovalent selective ion-exchange membranes. Science of the total environment, 722, p.137681.

[12] Ozairi, N., Mousavi, S.A., Samadi, M.T., Seidmohammadi, A. and Nayeri, D., 2020. Removal of fluoride from water using coagulation-flocculation process: a comparative study. Desalin. Water Treat., 180, pp.265-270.

[13] Fito, J., Said, H., Feleke, S. and Worku, A., 2019. Fluoride removal from aqueous solution onto activated carbon of Catha edulis through the adsorption treatment technology. Environmental Systems Research, 8(1), pp.1-10.

[14] Bhaumik, M., Leswifi, T.Y., Maity, A., Srinivasu, V.V. and Onyango, M.S., 2011. Removal of fluoride from aqueous solution by polypyrrole/Fe3O4 magnetic nanocomposite. Journal of hazardous materials, 186(1), pp.150-159.

[15] Chai, L., Wang, Y., Zhao, N., Yang, W. and You, X., 2013. Sulfate-doped Fe3O4/Al2O3 nanoparticles as a novel adsorbent for fluoride removal from drinking water. Water research, 47(12), pp.4040-4049.

[16] Abharya, A. and Gholizadeh, A., 2021. Synthesis of a Fe3O4-rGO-ZnO-catalyzed photo-Fenton system with enhanced photocatalytic performance. Ceramics International, 47(9), pp.12010-12019.

[17] Abharya, A. and Gholizadeh, A., 2020. Structural, optical and magnetic feature of core-shell nanostructured Fe3O4@ GO in photocatalytic activity. Iran. J. Chem. Chem. Eng. Research Article Vol, 39(2).

[18] Sihag, S. and Pal, J., 2023. Synthesis and characterization of zinc oxide nanocomposite for fluoride ion removal from aqueous solution. Environmental Monitoring and Assessment, 195(10), p.1205.

[19] Sarma, G.K., Sharma, R., Saikia, R., Borgohain, X., Iraqui, S., Bhattacharyya, K.G. and Rashid, M.H., 2020. Facile synthesis of chitosan-modified ZnO/ZnFe 2 O 4 nanocomposites for effective remediation of groundwater fluoride. Environmental Science and Pollution Research, 27, pp.30067-30080.

[20] Roychowdhury, A., Pati, S.P., Mishra, A.K., Kumar, S. and Das, D., 2013. Magnetically addressable fluorescent Fe_3O_4/ZnO nanocomposites: structural, optical and magnetization studies. Journal of Physics and Chemistry of Solids, 74(6), pp.811-818.

[21] Si, R., Zhang, Y.W., Li, S.J., Lin, B.X. and Yan, C.H., 2004. Urea-Based Hydrothermally Derived Homogeneous Nanostructured $Ce_{1-x}Zr_xO_2$ (x= 0− 0.8) Solid Solutions: A Strong Correlation between Oxygen Storage Capacity and Lattice Strain. The Journal of Physical Chemistry B, 108(33), pp.12481-12488.

[22] Irandoust, R. and Gholizadeh, A., 2020. A comparative study of the effect of the non-magnetic and magnetic trivalent rare-earth ion substitutions on bismuth ferrite properties: Correlation between the crystal structure and physical properties. Solid State Sciences, 101, p.106142.

[23] Gholizadeh, A., 2017. A comparative study of physical properties in Fe_3O_4 nanoparticles prepared by coprecipitation and citrate methods. Journal of the american ceramic society, 100(8), pp.3577-3588.

[24] Elmahaishi, M.F., Ismail, I. and Muhammad, F.D., 2022. A review on electromagnetic microwave absorption properties: their materials and performance. Journal of Materials Research and Technology, 20, pp.2188-2220.

[25] Mojahed, M., Dizaji, H.R. and Gholizadeh, A., 2022. Structural, magnetic, and dielectric properties of Ni/Zn co-

substituted CuFe2O4 nanoparticles. Physica B: Condensed Matter, 646, p.414337.

[26] Hashim, M., Kumar, S., Shirsath, S.E., Kotnala, R.K., Shah, J. and Kumar, R., 2013. Synthesis and characterizations of Ni^{2+} substituted cobalt ferrite nanoparticles. Materials Chemistry and Physics, 139(2-3), pp.364-374.

[27] Saffari, F., Kameli, P., Rahimi, M., Ahmadvand, H. and Salamati, H., 2015. Effects of Co-substitution on the structural and magnetic properties of $NiCoxFe_2- xO_4$ ferrite nanoparticles. Ceramics International, 41(6), pp.7352-7358.